Bowl-Shaped Radicals

DOI: 10.1002/anie.201002626

A Bowl-Shaped *ortho*-Semiquinone Radical Anion: Quantitative Evaluation of the Dynamic Behavior of Structural and Electronic Features**

Akira Ueda, Kanako Ogasawara, Shinsuke Nishida, Tomoaki Ise, Tomohiro Yoshino, Shigeaki Nakazawa, Kazunobu Sato, Takeji Takui, Kazuhiro Nakasuji, and Yasushi Morita**

Organic radical ions play increasingly important roles in a wide range of research fields from biochemistry to materials science.[1] *o*-Semiquinone is a typical organic radical anion with multistage redox ability that can form chelate salts and complexes with many kinds of metal cations. Investigation of a variety of transition-metal complexes of *o*-semiquinone radical could help not only to increase general knowledge of their fundamental chemistry but also to develop functional materials based on valence tautomerism phenomena.[2,3] In contrast, the alkali-metal salts have been extensively studied, and much attention has been focused on the dynamic behavior of their structure and of the electronic features of the ion pair in solution.[4,5] Solution-phase ESR spectroscopy measurements of some alkali-metal salts show significant temperature dependence in their hyperfine coupling constants (hfccs).[4b,d] The origin of this behavior has been only qualitatively interpreted as temperature-dependent positional change or migration of the alkali-metal cation to the oxygen atoms of the *o*-semiquinone radical.[4e,h] A quantitative discussion of such dynamic behavior has not been carried out to date.

Recently, we synthesized and isolated corannulene (**1**)[6]-based stable neutral mono- and diradical derivatives with bowl-shaped non-alternant π-conjugated systems.[7] Their three-dimensional spin-delocalized nature and intra- and intermolecular magnetic interactions were experimentally illustrated in terms of geometrical and topological aspects. These studies have inspired us to design a novel bowl-shaped radical anion system $\mathbf{2}^{\bullet-}$ based on corannulene with the *o*-semiquinone moiety. Notably, $\mathbf{2}^{\bullet-}$ is the first bowl-shaped semiquinone radical anion with non-alternant π conjugation.[8] Herein we report the synthesis of a sodium salt of $\mathbf{2}^{\bullet-}$ ($Na^+\cdot\mathbf{2}^{\bullet-}$), which is stable in an oxygen-free solution and even in the solid state under nitrogen atmosphere. Thanks to the high stability imparted by the bulky *tert*-butyl groups, we could evaluate 3D molecular and electronic structures of $Na^+\cdot\mathbf{2}^{\bullet-}$ using the curvature and electronic spin and charge distribution by ESR spectroscopy and ^1H and ^{23}Na ENDOR/TRIPLE measurements as well as by DFT calculations. We emphasize that the temperature dependence of the hfccs, related to the bowl-shaped structure, can for the first time allow for a quantitative discussion of the dynamic behavior of the ion pair in a solution of $Na^+\cdot\mathbf{2}^{\bullet-}$ with the help of sophisticated DFT calculations. These studies demonstrate the salient structural and electronic features of a bowl-shaped semiquinone radical salt with the temperature-dependent positional change of a countercation, which originates in the concave–convex dynamics of the bowl-shaped skeleton.

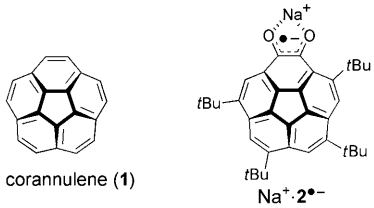

A synthetic route for $Na^+\cdot\mathbf{2}^{\bullet-}$ is depicted in Scheme 1. Our modified experimental conditions of the reported penta-*tert*-butylation of **1**[9] gave tetra-*tert*-butyl corannulene **3** as the major product. By bromination and subsequent coupling reaction,[10] we obtained the silyl ether derivative **5**. The quinone **7**, a semiquinone radical precursor, was obtained as red-orange plates[11] by desilylation of **5** and subsequent oxidation. Treatment of **7** with a sodium mirror in an oxygen-free 2-methyl-THF solution gave $Na^+\cdot\mathbf{2}^{\bullet-}$ as a deep blue

[*] Dr. A. Ueda, K. Ogasawara, Prof. Dr. K. Nakasuji, Prof. Dr. Y. Morita
Department of Chemistry
Graduate School of Science, Osaka University
Toyonaka, Osaka 560-0043 (Japan)
Fax: (+81) 6-6850-5395
E-mail: morita@chem.sci.osaka-u.ac.jp
Homepage: http://www.chem.sci.osaka-u.ac.jp/lab/nakasuji/morita/index_eng.html
Dr. S. Nishida, Dr. T. Ise, T. Yoshino, Dr. S. Nakazawa, Prof. Dr. K. Sato, Prof. Dr. T. Takui
Department of Chemistry and Materials Science
Graduate School of Science, Osaka City University
Sumiyoshi-ku Osaka 558-8585 (Japan)
Fax: (+81) 6-6605-2522
E-mail: takui@sci.osaka-cu.ac.jp
Homepage: http://www.qcqis.sci.osaka-cu.ac.jp/english/index.html

[**] This work was partially supported by a Grant-in-Aid for Scientific Research on Innovative Areas (No. 20110006) from the Ministry of Education, Culture, Sports, Science and Technology (Japan), the Global COE Program "Global Education and Research Center for Bio-Environmental Chemistry" of Osaka University, and CREST-JST (Japan). A.U. is a recipient of a Japan Society for the Promotion of Science (JSPS) research fellowship.

Supporting information for this article is available on the WWW under http://dx.doi.org/10.1002/anie.201002626.

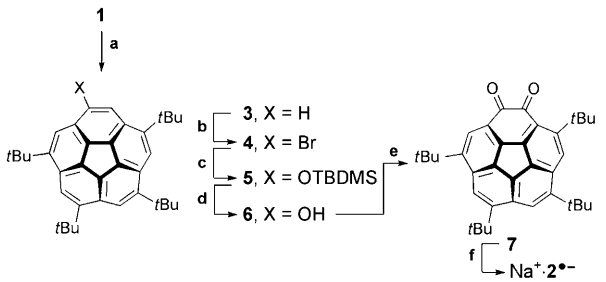

Scheme 1. Synthesis of $Na^{+}\cdot\mathbf{2}^{\bullet-}$: a) *t*BuCl, $AlCl_3$, 0 °C, 62% (estimated by ^{1}H NMR spectroscopy); b) Br_2, $FeBr_3$, CH_2Cl_2, −78 °C, 98% (estimated by ^{1}H NMR spectroscopy); c) NaOTBDMS, $[Pd(dba)_2]$, (*S*)-Tol-BINAP, toluene, 120 °C, 45% (estimated by ^{1}H NMR spectroscopy); d) Bu_4NF, THF, room temperature, 100%; e) Ag_2O, toluene, 90 °C, 21%; f) sodium mirror, 2-methyl-THF, room temperature. TBDMS = *tert*-butyldimethylsilyl, dba = dibenzylideneacetone, (*S*)-Tol-BINAP = (*S*)-(−)-2,2′-bis(di-*p*-tolylphosphino)-1,1′-binaphthyl.

solution. This salt is very stable in an oxygen-free solution and is also stable in the solid state under nitrogen atmosphere.[12]

To evaluate the electronic-spin structure of $Na^{+}\cdot\mathbf{2}^{\bullet-}$ in solution, we carried out ESR spectroscopy and ^{1}H and ^{23}Na ENDOR/TRIPLE measurements in an oxygen-free 2-methyl-THF solution. An ESR spectrum at 270 K shows eight hyperfine splittings ($g = 2.0044$, Figure 1a). Hfccs and their relative signs at 270 K were unequivocally determined by ^{1}H and ^{23}Na ENDOR/TRIPLE spectroscopy (Figure 1b).[13] Assignment of the hfccs was achieved with the help of DFT calculations (Table 1, Figure 2a).[14] Observed

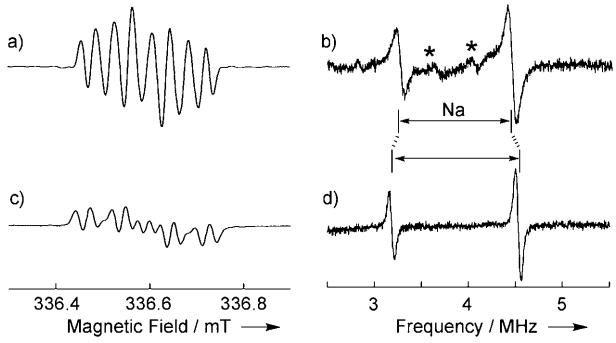

Figure 1. Observed a) ESR (microwave frequency: 9.44283 GHz) and b) ^{23}Na ENDOR spectra at 270 K and c) ESR (microwave frequency: 9.44284 GHz) and d) ^{23}Na ENDOR spectra at 210 K for $Na^{+}\cdot\mathbf{2}^{\bullet-}$ in an oxygen-free 2-methyl-THF solution (5×10^{-3} M). Asterisks denote spurious noise arising from strong RF irradiation.

proton hfccs are in good agreement with the calculated ones for the optimized structure of $Na^{+}\cdot\mathbf{2}^{\bullet-}$, in which the sodium cation is located in the semiquinone plane and is chelated by the two oxygen atoms. However, the experimentally obtained hfcc of the Na nucleus deviates significantly from the calculated one (Table 1, see below). These ESR spectroscopy experiments demonstrate extensive spin delocalization on the curved π surface of $\mathbf{2}^{\bullet-}$ (Figure 2a). The sum of the absolute spin density on the corannulene skeleton of $Na^{+}\cdot\mathbf{2}^{\bullet-}$ (0.880) is

Table 1: Experimental and calculated hyperfine coupling constants (hfccs, in mT) of $Na^{+}\cdot\mathbf{2}^{\bullet-}$.

	H6	H8	H10	H(*t*Bu)	Na
Obsd (270 K)[a]	−0.075	+0.035	−0.026	+0.005	−0.042
Obsd (210 K)[a]	−0.075	+0.034	−0.025	+0.005	−0.048
Calcd[b]	−0.071	+0.031	−0.030	+0.006	−0.123

[a] Values and relative signs were determined by ^{1}H and ^{23}Na ENDOR/TRIPLE spectra. [b] Hfccs of the optimized structure calculated at the UBLYP/6-31G(d,p) level of theory.

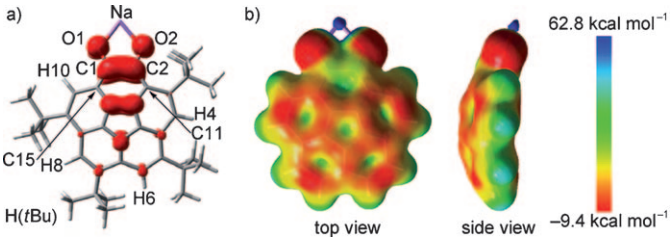

Figure 2. a) Spin density distribution of $Na^{+}\cdot\mathbf{2}^{\bullet-}$ and b) electrostatic potential surfaces of $Na^{+}\cdot\mathbf{2}^{\bullet-}$ (unsubstituted) calculated at the UBLYP/6-31G(d,p) level of theory. The red color in (a) denotes positive spin density. The blue and red regions in (b) represent large positive and negative charge distributions, respectively.

much larger than that of the corannulene-based neutral monoradical derivatives bearing the phenoxyl (0.553),[7c] verdazyl (0.241),[7a] or iminonitroxide (0.175)[7b] moiety. Noticeably, the delocalized spin density of $Na^{+}\cdot\mathbf{2}^{\bullet-}$ is distributed in a C_2 symmetrical fashion, in contrast to the unbalanced spin-delocalized nature of the neutral monoradical systems.[7a–c] There are sizable amounts of spin density in the central five-membered ring of $\mathbf{2}^{\bullet-}$, which implies a significant contribution of the cyclopentadienyl radical structure as well as the semiquinone radical one. This unique spin delocalization is attributable to the topological nature of the non-alternant π conjugation of $\mathbf{2}^{\bullet-}$. Electrostatic potential surfaces of $Na^{+}\cdot\mathbf{2}^{\bullet-}$ (Figure 2b) indicate that negative charge densities are delocalized not only on the two oxygen atoms but also over the whole curved π network. In contrast to the negative charge, the positive charge is localized on the Na atom.

To obtain information on the structural features of this system, we examined the curvature of $\mathbf{2}^{\bullet-}$ and its redox species, neutral quinone **7** and dianion derivatives,[15] by DFT calculations using the crystal structure of **7** as an initial structure. Interestingly, the curvature of the studied species deepens in a stepwise fashion with increasing negative charge.[16] This finding is in sharp contrast to the parent corannulene **1** and phenalenyl-fused corannulene systems.[17] This curvature deepening in the present system is probably due to the increase in the tethering tendency of the bowl-shaped skeleton by the decrease of the C1–C2, C1–C15, and C2–C11 bond lengths with reduction.[18]

To gain insight into the origin of the difference between the experimental and theoretical hfcc of the Na nucleus (A^{Na}), we focused on dynamic behavior of $Na^{+}\cdot\mathbf{2}^{\bullet-}$ in solution. The variable-temperature ESR spectroscopy measurements using

dual-sample-port cavity equipment demonstrated that the g value and signal intensity at 210 K are identical to those at 270 K (Figure 3).[13,19] However, the line shapes of the ESR spectra differ significantly (Figure 1 a,c). Interestingly, the

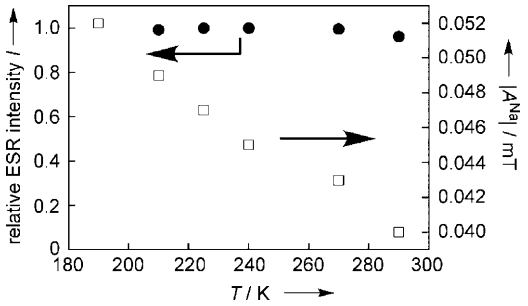

Figure 3. Temperature dependence of the relative ESR intensity (I, ●, left) and magnitude of hfcc of the Na nucleus ($|A^{Na}|$, □, right) for $Na^+\cdot\mathbf{2}^{\bullet-}$. The relative ESR intensity I represents the ratio of the ESR intensities of $Na^+\cdot\mathbf{2}^{\bullet-}$ and DPPH (1,1-diphenyl-2-picrylhydrazyl) measured under the same conditions (temperature, microwave frequency, and Q value).[19] The $|A^{Na}|$ values were obtained by ESR spectral simulation.[20]

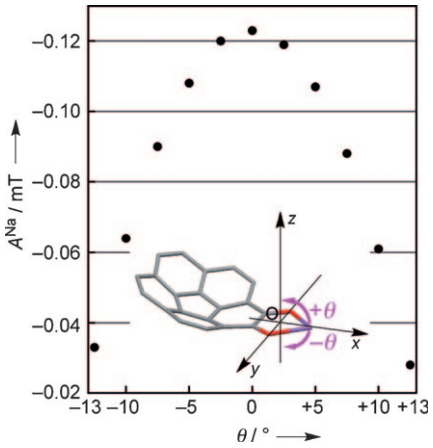

Figure 4. Calculated hfcc of the Na nucleus (A^{Na}, ●) for $Na^+\cdot\mathbf{2}^{\bullet-}$ depending on θ, which is the angle between the x axis and the line connecting the Na cation with the origin O. The distance between the Na cation and each oxygen atom is constant. Positive and negative θ values mean that the Na cation is in the concave and convex sides, respectively. The calculations were carried out at the UBLYP/6-31G-(d,p) level of theory. In the inset, *tert*-butyl groups are omitted for clarity.

variable-temperature ^1H and ^{23}Na ENDOR/TRIPLE measurements (Figure 1 b,d)[13] indicate that A^{Na} becomes more negative with lowering temperature while hfccs of the protons are unchanged (Table 1). The ESR spectral simulation[20] showed that the line-shape change is due to only the temperature-dependent A^{Na} value. To gain in-depth knowledge about this temperature-dependent behavior, we carried out additional ESR spectroscopy measurements of $Na^+\cdot\mathbf{2}^{\bullet-}$ at 190, 225, 240, and 290 K in solution.[13] The ESR spectral simulations[20] indicate that the absolute value $|A^{Na}|$ increases with lowering temperature (Figure 3)[21] and gradually approaches the value of the optimized structure (0.123 mT in Table 1). These experimental results suggest the following points: 1) The temperature-dependent change in A^{Na} is due to the positional change of the Na cation relative to $\mathbf{2}^{\bullet-}$. 2) With decreasing temperature, the position comes closer to that of the optimized structure. 3) Therefore, the experimental A^{Na} value at 270 K is significantly different from the calculated one of the optimized structure, while the experimental hfccs of the protons at 270 K are in good agreement with the calculated ones (Table 1).

To gain insight into the above temperature-dependent behavior, we calculated A^{Na} of $Na^+\cdot\mathbf{2}^{\bullet-}$ for defined positions of the Na cation relative to $\mathbf{2}^{\bullet-}$ by the DFT method. We set up x, y, and z axes and angle θ (see inset of Figure 4)[22] to define the position of the Na cation. For the positional change of the Na cation, we focused on the motion in the xz plane, keeping a constant distance between the Na cation and each oxygen atom. Depending on θ, the Na cation moves to the convex or the concave side of $\mathbf{2}^{\bullet-}$. Figure 4 shows the angular (θ) dependence of the calculated A^{Na} value of $Na^+\cdot\mathbf{2}^{\bullet-}$. When the angle θ is 0°, that is, the sodium cation is in the xy plane, $|A^{Na}|$ takes the maximum. As the sodium cation departs from the xy plane, $|A^{Na}|$ gradually decreases.[23] Notably, the experimentally obtained $|A^{Na}|$ values (0.040 to ca. 0.052 mT, Figure 3) are similar to the calculated ones with the angle θ in the range of $+10$ and $+12.5°$ or -10 and $-12.5°$ (Figure 4). This finding means that the Na cation is not in the xy plane. Also, the increase of the experimental $|A^{Na}|$ value with decreasing temperature (Table 1, Figure 3) corresponds to the decrease of θ in this model. Another possible model based on the positional change of the sodium cation on the x axis does not reproduce the temperature-dependence of $|A^{Na}|$.[24] Therefore, we have concluded that the sodium cation approaches the xy plane or the O-C-C-O plane with decreasing temperature. Figure 4 provides another interesting point for the angular dependence of A^{Na} in this system. An $|A^{Na}|$ value for negative θ is always larger than that for the corresponding positive θ value; for example, $|A^{Na}| = 0.064$ mT ($\theta = -10°$) and $|A^{Na}| = 0.061$ mT ($\theta = +10°$). This difference is clearly due to the intrinsically 3D structure of $\mathbf{2}^{\bullet-}$, in which the π-electronic system of the convex and concave sides are asymmetrically related to each other.[25] Furthermore, the DFT calculations of some sodium salts of corannulene-based semiquinone radicals with different curvatures suggest that the difference of $|A^{Na}|$ in each side becomes significantly larger with increasing curvature of the bowl-shaped skeleton.[26]

In summary, the first bowl-shaped semiquinone radical salt $Na^+\cdot\mathbf{2}^{\bullet-}$ has been synthesized, and its 3D spin- and charge-delocalized natures and redox properties have been characterized. Especially, we emphasize the quantitative evaluation of the convex–concave dynamic behavior, which originates in the structural and electronic features of the curved π radical $\mathbf{2}^{\bullet-}$. This bowl-shaped skeleton has an intermediate geometry between planar π radical[27,28] and tetrahedral σ radical. At the present stage, we assume that this dynamic behavior is attributable to the temperature-dependent influence of solvation[5d] and thermal motion of the ion pair, thus allowing a reasonable interpretation of the variable A^{Na} values with the

help of state-of-the-art quantum chemical computations. These findings demonstrate that this class of *o*-semiquinone radical salts with curved π-conjugated systems is an intriguing model system not only for studying the dynamic behavior of the ion pair but also for gaining molecular-level information on the electronic structure of convex and concave faces in a curved open-shell system by the use the countercation as a probe. Taking advantage of the high stability and chelating ability of $\mathbf{2}^{\bullet-}$, we are currently investigating chelating complexes with paramagnetic metal ions. Intra- and intermolecular magnetic interactions and valence tautomerism phenomena of metal–organic hybrid systems in curved π-conjugated radical ion species are of great interest for developing molecule-based functional materials displaying 3D spin and charge delocalization in the solid state and electronic-spin structures associated with the dynamic behavior in the solution state.[3,29–32]

Received: May 1, 2010
Published online: July 26, 2010

Keywords: corannulenes · EPR spectroscopy · ion pairs · radical ions · semiquinone

[1] a) *Radical Ions* (Eds.: E. T. Kaiser, L. Kevan), Interscience, New York, **1968**; b) N. L. Bauld, *Radicals, Ion Radicals, and Triplets*, Wiley-VCH, Weinheim, **1997**; c) Z. V. Todres, *Organic Ion Radicals: Chemistry and Applications*, Marcel Dekker, New York, **2003**; d) *Radical and Radical Ion Reactivity in Nucleic Acid Chemistry* (Ed.: M. M. Greenberg), Wiley, New Jersey, **2009**.

[2] a) C. G. Pierpont, R. M. Buchanan, *Coord. Chem. Rev.* **1981**, *38*, 45–87; b) W. Kaim, *Coord. Chem. Rev.* **1987**, *76*, 187–235.

[3] Various kinds of transition-metal (Co, Mn, Cu, Fe, etc.) complexes of *o*-semiquinone radicals exhibit valence tautomerism accompanying phase transition. This behavior is in contrast to a continuous positional change of a metal cation in the alkali-metal salts (reference [4,5]); a) R. M. Buchanan, C. G. Pierpont, *J. Am. Chem. Soc.* **1980**, *102*, 4951–4957; b) D. M. Adams, A. Dei, A. L. Rheingold, D. N. Hendrickson, *J. Am. Chem. Soc.* **1993**, *115*, 8221–8229; c) D. A. Shultz in *Magnetism: Molecules to Materials II* (Eds.: J. S. Miller, M. Drillon), Wiley-VCH, Weinheim, **1997**, pp. 281–306; d) C. G. Pierpont, *Coord. Chem. Rev.* **2001**, *216–217*, 99–125; e) A. Dei, D. Gatteschi, C. Sangregorio, L. Sorace, *Acc. Chem. Res.* **2004**, *37*, 827–835; f) O. Sato, A. Cui, R. Matsuda, J. Tao, S. Hayami, *Acc. Chem. Res.* **2007**, *40*, 361–369; g) O. Sato, J. Tao, Y.-Z. Zhang, *Angew. Chem.* **2007**, *119*, 2200–2236; *Angew. Chem. Int. Ed.* **2007**, *46*, 2152–2187.

[4] a) D. R. Eaton, *Inorg. Chem.* **1964**, *3*, 1268–1271; b) E. Warhurst, A. M. Wilde, *Trans. Faraday Soc.* **1969**, *65*, 1413–1418; c) J. Pilar, *J. Phys. Chem.* **1970**, *74*, 4029–4037; d) Pasimeni, C. Corvaja, *J. Chem. Soc. Faraday Trans. 2* **1975**, *71*, 193–200; e) L. Pasimeni, M. Brustolon, C. Corvaja, *J. Magn. Reson.* **1976**, *21*, 259–269; f) C. C. Felix, R. C. Sealy, *J. Am. Chem. Soc.* **1982**, *104*, 1555–1560; g) H. Bock, D. Jaculi, *Angew. Chem.* **1984**, *96*, 298–299; *Angew. Chem. Int. Ed. Engl.* **1984**, *23*, 305–307; h) Y. Shinagawa, Y. Shinagawa, *Int. J. Quantum Chem.* **1986**, *29*, 361–371; i) H. Kurreck, B. Kirste, W. Lubitz, *Electron Nuclear Double Resonance Spectroscopy of Radicals in Solution*, Wiley-VCH, New York, **1988**, pp. 111–208.

[5] *Ions and Ion Pairs in Organic Reactions, Vol. 1 and 2* (Ed.: M. Szwarc), Wiley Interscience, New York, **1972** and **1974**.

[6] a) R. E. Barth, R. G. Lawton, *J. Am. Chem. Soc.* **1966**, *88*, 380–381. For recent reviews on corannulene and related compounds, see: b) A. Sygula, P. W. Rabideau in *Carbon-Rich Compounds*, (Eds.: M. M. Haley, R. R. Tykwinski), Wiley-VCH, Weinheim, **2006**, pp. 529–565; c) Y.-T. Wu, J. S. Siegel, *Chem. Rev.* **2006**, *106*, 4843–4867; d) V. M. Tsefrikas, L. T. Scott, *Chem. Rev.* **2006**, *106*, 4868–4884.

[7] a) Y. Morita, S. Nishida, T. Kobayashi, K. Fukui, K. Sato, D. Shiomi, T. Takui, K. Nakasuji, *Org. Lett.* **2004**, *6*, 1397–1400; b) S. Nishida, Y. Morita, T. Kobayashi, K. Fukui, A. Ueda, K. Sato, D. Shiomi, T. Takui, K. Nakasuji, *Polyhedron* **2005**, *24*, 2200–2204; c) Y. Morita, A. Ueda, S. Nishida, K. Fukui, T. Ise, D. Shiomi, K. Sato, T. Takui, K. Nakasuji, *Angew. Chem.* **2008**, *120*, 2065–2068; *Angew. Chem. Int. Ed.* **2008**, *47*, 2035–2038; d) A. Ueda, S. Nishida, K. Fukui, T. Ise, D. Shiomi, K. Sato, T. Takui, K. Nakasuji, Y. Morita, *Angew. Chem.* **2010**, *122*, 1722–1726; *Angew. Chem. Int. Ed.* **2010**, *49*, 1678–1682.

[8] Radical mono- and trianion species of **1** were generated by chemical reduction in solution in a sealed tube and were detected by ESR spectroscopy measurements. However, their isolation was not performed. See a) J. Janata, J. Gendell, C.-Y. Ling, W. Barth, L. Backes, H. B. Mark, Jr., R. G. Lawton, *J. Am. Chem. Soc.* **1967**, *89*, 3056–3058; b) M. Baumgarten, L. Gherghel, M. Wagner, A. Weitz, M. Rabinovitz, P.-C. Cheng, L. T. Scott, *J. Am. Chem. Soc.* **1995**, *117*, 6254–6257; c) G. Zilber, V. Rozenshtein, P.-C. Cheng, L. T. Scott, M. Rabinovitz, H. Levanon, *J. Am. Chem. Soc.* **1995**, *117*, 10720–10725. Scott, Rabinovitz, and co-workers reported the reduction of several corannulene derivatives having annelated six- or five-membered rings. The closed-shell anions were characterized by NMR spectroscopy, however the open-shell ones were not detected. See d) A. Weitz, E. Shabtai, M. Rabinovitz, M. S. Bratcher, C. C. McComas, M. D. Best, L. T. Scott, *Chem. Eur. J.* **1998**, *4*, 234–239; e) I. Aprahamian, R. E. Hoffman, T. Sheradsky, D. V. Preda, M. Bancu, L. T. Scott, M. Rabinovitz, *Angew. Chem.* **2002**, *114*, 1788–1791; *Angew. Chem. Int. Ed.* **2002**, *41*, 1712–1715; f) I. Aprahamian, D. V. Preda, M. Bancu, A. P. Belanger, T. Sheradsky, L. T. Scott, M. Rabinovitz, *J. Org. Chem.* **2006**, *71*, 290–298.

[9] a) P.-C. Cheng, Ph.D. Thesis, Boston College, **1996**; b) Y. Sevryugina, A. Y. Rogachev, E. A. Jackson, L. T. Scott, M. A. Petrukhina, *J. Org. Chem.* **2006**, *71*, 6615–6618.

[10] G. Mann, J. F. Hartwig, *J. Org. Chem.* **1997**, *62*, 5413–5418.

[11] The quinone derivative **7** forms convex–convex type dimeric pairs in the crystal. To our knowledge, this is the first convex–convex type crystal structure in bowl-shaped π-conjugated molecules. For details, see the Supporting Information.

[12] The stability of the samples was judged from the signal intensity of their solution ESR spectra.

[13] Experimentally, we could not explicitly detect the hyperfine splitting attributable to H4 in ^{1}H ENDOR/TRIPLE spectra. Considering that the hfcc of H4 is expected to be much smaller (−0.001 mT) than that of H(*t*Bu) on the basis of DFT calculations (UBLYP/6-31G(d,p)), the ^{1}H ENDOR/TRIPLE signals arising from H4 are masked by the strong signals of the protons of H(*t*Bu) (Figure S18 in the Supporting Information). All recorded ESR and ^{1}H and ^{23}Na ENDOR/TRIPLE spectra are shown in the Supporting Information.

[14] All DFT calculations were performed with the Gaussian03 program (revision E.01) Gaussian, Inc., Wallingford CT, 2004; the full reference is given in the Supporting Information.

[15] Cyclic voltammetry of **7** shows two irreversible reduction waves at −1.14 and −1.95 V (vs ferrocene/ferrocenium), indicating the electrochemical generation of the semiquinone radical $\mathbf{2}^{\bullet-}$ and the dianion species. The voltammogram is given in the Supporting Information.

[16] The average POAV (π orbital axis vector) angle in the central five-membered ring and the bowl depth are 5.3° and 0.55 Å for the neutral quinone **7**, 6.0° and 0.64 Å for $\mathbf{2}^{\bullet-}$, and 6.3° and 0.67 Å for the dianion, respectively. The detailed data are described in the Supporting Information.

[17] On the basis of theory it is suggested that their curvature shallows in a stepwise manner with increasing negative charge. For **1**, see: a) C. Bruno, R. Benassi, A. Passalacqua, F. Paolucci, C. Fontanesi, M. Marcaccio, E. A. Jackson, L. T. Scott, *J. Phys. Chem. B* **2009**, *113*, 1954–1962. For the phenalenyl-fused corannulene, see: b) S. Nishida, Y. Morita, A. Ueda, T. Kobayashi, K. Fukui, K. Ogasawara, K. Sato, T. Takui, K. Nakasuji, *J. Am. Chem. Soc.* **2008**, *130*, 14954–14955.

[18] The details of bond-length analyses and resonance structures of these redox species are shown in the Supporting Information.

[19] The temperature dependence of the ESR intensity is given in the Supporting Information. The absolute concentration of the radical was accurately measured by exploiting a dual-sample-port cavity.

[20] The simulated ESR spectra and hfccs are shown in the Supporting Information.

[21] The trend of temperature-dependent $|A^{Na}|$ change of $Na^{+}\cdot\mathbf{2}^{\bullet-}$ is similar to that of several alkali-metal salts of an *o*-benzosemiquinone radical (see reference [4d]). In contrast, the magnitude of hfcc of an alkali-metal counterion of fluorenone ketyl or *p*-benzosemiquinone radical salts decreases with decreasing temperature. See a) N. Hirota, *J. Am. Chem. Soc.* **1967**, *89*, 32–41; b) M. P. Khakhar, B. S. Prabhananda, M. R. Das, *J. Am. Chem. Soc.* **1967**, *89*, 3100–3106. See also references [4, 5].

[22] The *y* axis is the line passing through the two oxygen atoms (shown in red), and the *xy* plane is coplanar with the semiquinone moiety. The *z* axis is perpendicular to the *xy* plane and passes through the origin O. The parameter θ represents the angle between the *x* axis and the line connecting the sodium cation with the origin O. Positive and negative θ values mean that the sodium cation is in the concave and convex sides, respectively.

[23] The calculated hfccs of protons are unchanged without angular dependence.

[24] The $|A^{Na}|$ change when the sodium cation moves on the *x* axis was examined by DFT calculations. For details, see the Supporting Information.

[25] This situation is in contrast to a planar *o*-benzosemiquinone radical salt without such sign dependence of θ.

[26] For example, $|A^{Na}|$ of acecorannulene semiquinone (bowl depth = 1.04 Å) salt are 0.109 mT ($\theta = -10°$) and 0.040 mT ($\theta = +10°$), showing a larger difference than those of $Na^{+}\cdot\mathbf{2}^{\bullet-}$ (0.064 and 0.061 mT; bowl depth = 0.62 Å). For details, see the Supporting Information.

[27] For our recent studies on planar neutral π radicals based on phenalenyl and oxophenalenoxyl systems, see: a) S. Nishida, Y. Morita, K. Fukui, K. Sato, D. Shiomi, T. Takui, K. Nakasuji, *Angew. Chem.* **2005**, *117*, 7443–7446; *Angew. Chem. Int. Ed.* **2005**, *44*, 7277–7280; b) S. Suzuki, Y. Morita, K. Fukui, K. Sato, D. Shiomi, T. Takui, K. Nakasuji, *J. Am. Chem. Soc.* **2006**, *128*, 2530–2531; c) Y. Morita, S. Suzuki, K. Fukui, S. Nakazawa, H. Kitagawa, H. Okamoto, A. Naito, A. Sekine, Y. Ohashi, M. Shiro, K. Sasaki, D. Shiomi, K. Sato, T. Takui, K. Nakasuji, *Nat. Mater.* **2008**, *7*, 48–51; d) Y. Morita, S. Nishida, J. Kawai, T. Takui, K. Nakasuji, *Pure Appl. Chem.* **2008**, *80*, 3988–3990.

[28] For a review of recent phenalenyl chemistry, see: "Phenalenyls, Cyclopentadienyls, and Other Carbon-Centered Radicals": Y. Morita, S. Nishida in *Stable Radicals: Fundamentals and Applied Aspects of Odd-electron Compounds* (Ed.: R. Hicks), Wiley-Blackwell, in press.

[29] a) *Magnetic Properties of Organic Materials* (Ed.: P. M. Lahti), Marcel Dekker, New York, **1999**; b) *Molecular Magnetism* (Eds.: K. Itoh, M. Kinoshita), Kodansha & Gordon and Breach, Tokyo, **2000**; c) *Molecular Magnets: Recent Highlights* (Eds.: W. Linert, M. Verdaguer), Springer, Wien, **2003**.

[30] Metal complexes of bowl-shaped π-conjugated molecules have been extensively studied for corannulene and sumanene derivatives. Most of them are closed-shell systems, and electronic-spin structure and magnetic properties are not revealed. See a) M. A. Petrukhina, L. T. Scott, *Dalton Trans.* **2005**, 2969–2975; b) T. Amaya, W.-Z. Wang, H. Sakane, T. Moriuchi, T. Hirao, *Angew. Chem.* **2010**, *122*, 413–416; *Angew. Chem. Int. Ed.* **2010**, *49*, 403–406, and references cited therein.

[31] We are also studying salts and complexes of the unsubstituted $\mathbf{2}^{\bullet-}$. By decreasing steric hinderance, more effective intermolecular interaction than with the *tert*-butyl derivative $\mathbf{2}^{\bullet-}$ is expected.

[32] We have calculated the bowl-inversion energy barrier of the corannulene-based semiquinone radicals with different curvature using the Siegel equation (T. J. Seiders, K. K. Baldridge, G. H. Grube, J. S. Siegel, *J. Am. Chem. Soc.* **2001**, *123*, 517–525; see the Supporting Information). For further investigation of the inversion from the experimental side, variable-temperature NMR spectroscopy measurements and pulsed ESR spectroscopy for the direct observation of the dynamic molecular and electronic-spin structures are underway.

